Flinders
UNIVERSITY

The following article appeared as:

Holmes-Ross, H.L. and Lawrance, W.D., 2010. The dissociation of NO–Ar($\tilde{A}$) from around threshold to 200 cm^{-1} above threshold. Journal of Chemical Physics, 133, 014304.

and may be found at:
http://jcp.aip.org/resource/1/jcpsa6/v133/i1/p014304_s1

DOI: http://dx.doi.org/10.1063/1.3458911

The dissociation of NO–Ar() from around threshold to 200cm−1 above threshold

Heather L. Holmes-Ross and Warren D. Lawrance

Citation: J. Chem. Phys. **133**, 014304 (2010); doi: 10.1063/1.3458911
View online: http://dx.doi.org/10.1063/1.3458911
View Table of Contents: http://jcp.aip.org/resource/1/JCPSA6/v133/i1
Published by the American Institute of Physics.

The dissociation of NO–Ar($\tilde{A}$) from around threshold to 200 cm^{-1} above threshold

Heather L. Holmes-Ross and Warren D. Lawrance[a)]
School of Chemical and Physical Sciences, Flinders University, G.P.O. Box 2100, Adelaide, South Australia 5001, Australia

(Received 12 January 2010; accepted 10 June 2010; published online 7 July 2010)

We report an investigation of the dissociation of $\tilde{A}$ state NO–Ar at energies from 23 cm^{-1} below the dissociation energy to 200 cm^{-1} above. The NO product rotational distributions show population in states that are not accessible with the energy available for excitation from the NO ground state. This effect is observed at photon energies from below the dissociation energy up to approximately 100 cm^{-1} above it. Translational energy distributions, extracted from velocity map images of individual rotational levels of the NO product, reveal contributions from excitation of high energy NO–Ar $\tilde{X}$ states at all the excess energies probed, although this diminishes with increasing photon energy and is quite small at 200 cm^{-1}, the highest energy studied. These translational energy distributions show that there are contributions arising from population in vibrational levels up to the $\tilde{X}$ state dissociation energy. We propose that the reason such sparsely populated levels contribute to the observed dissociation is a considerable increase in the transition moment, via the Franck–Condon factor associated with these highly excited states, which arises because of the quite different geometries in the NO–Ar $\tilde{X}$ and $\tilde{A}$ states. This effect is likely to arise in other systems with similarly large geometry changes. © *2010 American Institute of Physics*. [doi:10.1063/1.3458911]

I. INTRODUCTION

The NO–Ar van der Waals complex has been studied for several decades because it provides a simple prototype for the investigation of dispersion interactions involving an open shell molecule. The NO–Ar $\tilde{A}\ ^2\Sigma \leftarrow \tilde{X}\ ^2\Pi$ electronic spectrum, first observed via fluorescence from the NO photodissociation product,[1] consists of a broad, structureless feature some 300–400 cm^{-1} wide peaking near 44 550 cm^{-1}, indicating a significant change in the van der Waals potential between the two electronic states. Thuis *et al.*[2] suggested that the $\tilde{X}$ state of the complex is T-shaped, and this was subsequently confirmed by Mills *et al.*[3] from radiofrequency and microwave spectra. In contrast, the $\tilde{A}$ state is linear,[4,5] with the most recent results revealing that the argon is situated adjacent to the nitrogen atom.[6]

Because of the large geometry change between the $\tilde{X}$ and $\tilde{A}$ states, transitions to the bound region near the origin are very weak and it was some time before they were observed. The first investigation of the bound-bound $\tilde{A}\ ^2\Sigma \leftarrow \tilde{X}\ ^2\Pi$ transition was of quite low resolution but revealed that structure was observable.[7] Subsequent studies with increased resolution[8,9] revealed several bands assignable to vibrational modes.[9] The NO–Ar $\tilde{A}-\tilde{X}$ origin was determined as 44 242.4 cm^{-1} and this, along with measurements of the dissociation onset, allowed $\tilde{A}$ and $\tilde{X}$ state dissociation energies of 44 and 88 cm^{-1}, respectively, to be obtained,[8] although, as discussed below, these values have recently been called into question.[10] The identification of the features observed in the bound-bound $\tilde{A}-\tilde{X}$ spectrum was achieved through the enhanced quality of later resonance enhanced multiphoton ionization (REMPI) experiments.[4,11] However, a recent report has found that the previous assignments of the spectral features are incorrect.[6] These authors suggest that a quantitative fit of the major spectral features may be achieved by application of scaled results of their theoretical model, and that this should be the focus of future work. We expect that the correct assignment of the NO–Ar spectrum will be determined in due course.

There are aspects of the $\tilde{A}$ state dissociation of the complex that have yet to be satisfactorily explained. Indeed, few studies of the dissociation dynamics have been reported. Sato *et al.*[12] reported the first NO product state distributions in a series of experiments with available energies, E_a (i.e., the energy above dissociation), in the range 200–500 cm^{-1}.[12] The distributions showed two maxima, with the N states (N is the sum of the molecular rotational angular momentum and the electron angular momentum) at which these maxima occur, proportional to the square root of the excess energy. The authors rationalize this behavior as being similar to the rotational rainbow phenomenon observed in inelastic collision experiments.[13]

Tsuji *et al.*[8] investigated the onset of dissociation by measuring action spectra for several NO N states. A significant outcome of their work was the observation of resonance features above dissociation for $N=1,2$. The authors described these as shape resonance absorption bands and proposed a barrier to dissociation. Because the resonances were not observed for $N=3$, they placed an upper limit of 24 cm^{-1}

[a)]Electronic mail: warren.lawrance@flinders.edu.au.

on the barrier height. Roeterdink *et al.*[10] have recently reported on a velocity map ion imaging (VMI) investigation of dissociation following excitation of the resonance features. They proposed that because the change in geometry associated with excitation to the $\tilde{A}$ state causes mixing between the ground and excited states of the complex, the resonance features can be attributed to a type of vibrational Feshbach effect and are not the result of a barrier to dissociation. A significant outcome of their investigation was an increase in the value for the dissociation energy. The authors found that the translational energy of the products following excitation of some predissociative resonances was higher than expected and they determined that this was because the features are associated with excitation from thermally populated levels of $\tilde{X}$ state NO–Ar. Their results identified those transitions from the lowest vibrational level of $\tilde{X}$. Their observations infer binding energies of 52 and 96 cm^{-1} in the $\tilde{A}$ and $\tilde{X}$ states, respectively.

Chandler's group[14] had earlier reported rotational distributions for the A state NO product following $\tilde{A} \leftarrow \tilde{X}$ photodissociation, extending the investigation of Sato *et al.*[12] to lower available energy. They acquired NO(A) N distributions for E_a in the range 25–400 cm^{-1}. Unexpectedly, their distributions for $E_a < 100$ cm^{-1} revealed population in NO rotational states that are not accessible with the energy available. They concluded that vibrational hotband absorption from NO–Ar $\tilde{X}$ states with energy up to 27 cm^{-1}, as assigned by Monti *et al.*,[15] contributes to the product NO rotational populations. They proposed that excitation from these thermally populated levels is weak near dissociation, becomes significant between $E_a = 25-100$ cm^{-1}, and does not contribute at higher available energies. The authors note such absorption behavior as curious and suggest that it may result from rapid changes in magnitude for the Franck–Condon factors in this region.

Recently, we reported[16] a VMI study of the energetically forbidden NO rotational products identified by Chandler's group, at $E_a = 50$ cm^{-1}. This study revealed unexpectedly large translational energies associated with all N states of the NO(A) product.

These recent studies[10,14,16] show that there is a contribution to the observed photodissociation arising from excitation from levels above the ground state. A particular issue requiring further investigation is the extent to which these thermally populated $\tilde{X}$ states contribute to the observed dissociation around threshold and at what point their influence can be ignored. We have measured the translational and rotational distributions for the NO products following excitation below, at, and above the accepted dissociation threshold. We here present the results of this investigation.

II. EXPERIMENTAL DETAILS

In overview, the experiments involve, as the first step, excitation of the NO–Ar $\tilde{A} \leftarrow \tilde{X}$ transition, which leads to dissociation of NO–Ar $\tilde{A}$ into NO(A) and Ar. A second laser probes the NO(A) products using 1+1 REMPI via either the forbidden $F\ ^2\Delta \leftarrow A\ ^2\Sigma$ or allowed $E\ ^2\Sigma \leftarrow A\ ^2\Sigma$ transition. The resulting ions are detected using a time of flight mass spectrometer, yielding REMPI spectra or NO N-specific VMIs. Generally, the R branch of the $E \leftarrow A$ transition is utilized to monitor NO(A) because the selection rules allow all NO N states to be probed, unlike the $F \leftarrow A$ transition. The $E \leftarrow A$ transition was also used by Parsons *et al.*,[14] providing direct comparison of results. Because the $E \leftarrow A$ transition is strongly allowed, it is easily saturated, causing broadening,[8,12] and we find it necessary to use very low probe laser intensity to minimize this problem.

The experimental apparatus has been detailed previously.[17] NO–Ar complexes are formed via supersonic expansion when a mixture of 5% NO in argon, at a backing pressure of 7 atm, is introduced into the vacuum chamber through the 0.3 mm orifice of a pulsed nozzle. The resulting expansion passes through a 1 mm skimmer into the extraction region of a time of flight mass spectrometer operating in velocity map imaging mode. The complexes are photodissociated using the ~225 nm, focused, frequency tripled output of a neodymium-doped yttrium aluminium garnet (Nd:YAG) pumped dye laser (frequency tripled line width of approximately 0.6 cm^{-1}; ~10 μJ/pulse). Depending on the transition, either the ~560 nm ($F \leftarrow A$) or ~600 nm ($E \leftarrow A$) output of a second Nd:YAG pumped dye laser (line width of approximately 0.4 cm^{-1}, ~130, or 500 μJ/pulse for the E or F states, respectively) ionizes the A state NO dissociation product. The wavelengths of both beams are verified using a Bristol 821 pulsed wavemeter. The probe pulse is delayed by 300 ns, allowing ions from this second step to be detected with no interference from ions generated by the initial dissociation pulse. As the $v=0$ A state lifetime is 205 ns,[18] using this delay the NO A concentration has decayed by ~77% before ionization. The ions produced are detected using a chevron pair of matched microchannel plates (MCPs) backed by a phosphor screen. NO^+ ions are selected by pulsing the front MCP on at the appropriate arrival time. A charge coupled device (CCD) camera with a video zoom lens takes an image of the phosphor screen each time the detector is pulsed. The experiment is operated at 10 Hz.

CCD images are downloaded to the data acquisition PC and analyzed shot-by-shot to accumulate a histogram of ion count versus detector position. This creates a two dimensional projection of the three dimensional velocity distribution. The three dimensional distribution is recreated by applying an Inverse Abel transform to the image.[17,19] An experimentally determined calibration factor is used to convert radial distance from the image center into energy, allowing the translation energy distribution to be extracted.

III. RESULTS

A. NO *A* rotational distributions

Rotational distributions have been measured for A state NO formed following photolysis at eight laser excitation positions: 44 264, 44 275, 44 287, 44 297, 44 312, 44 337, 44 387, and 44 487 cm^{-1}. As will be discussed in detail in Sec. IV B, these are associated with effective excess energies in NO–Ar of approximately −23, −12, 0, 10, 25, 50, 100, and 200 cm^{-1}, respectively. The distributions for photolysis

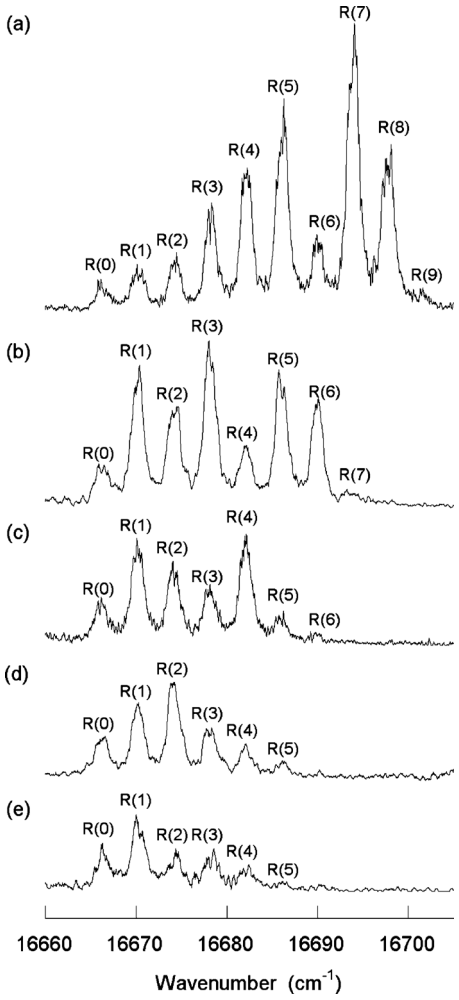

FIG. 1. REMPI spectra showing the R branch of the $E \leftarrow A$ transition for NO A products formed following photolysis of NO–Ar at the laser excitation positions (a) 44 487, (b) 44 387, (c) 44 337, (d) 44 312, and (e) 44 297 cm^{-1}. These are associated with effective excess energies in NO–Ar of approximately 200, 100, 50, 25, and 10 cm^{-1}, respectively. The R branch allows observation of all N; the P branch does not allow observation of $N=0$.

energies of 44 297 cm^{-1} and greater were determined from spectra of the R branch of the $E \leftarrow A$ transition; these spectra are shown in Fig. 1. The R branch is used as it allows observation of all N; the P branch does not allow observation of $N=0$. For the lower photolysis energies, interference in the spectra prevents use of the R branch, as shown in Fig. 2. This growth is ascribed to the following mechanism:

$$\mathrm{NO-Ar}(\tilde{X}) \xrightarrow{h\nu_{\mathrm{photolysis}}} \mathrm{NO-Ar}(\tilde{A}) \xrightarrow{h\nu_{\mathrm{probe}}} \mathrm{NO-Ar}(\tilde{E}),$$

$$\mathrm{NO-Ar}(\tilde{E}) \rightarrow \mathrm{Ar} + \mathrm{NO}(E),$$

$$\mathrm{NO}(E) \xrightarrow{h\nu_{\mathrm{probe}}} \mathrm{NO}^{+}.$$

Probe laser excitation of intact NO–Ar($\tilde{A}$) to above dissociation in the $\tilde{E}$ state produces NO(E) products which are subsequently ionized via absorption of a second probe laser photon, giving a background NO signal underlying the spectrum. For this mechanism to operate, the probe laser photon energy must exceed the energy required for excitation above the E state dissociation threshold. For photolysis at the NO–Ar($\tilde{A}$) dissociation threshold, the energy required to excite the complexes to the E state dissociation threshold is the NO $E-A$ energy gap, ΔE_{E-A}. For photolysis photon energies below the NO–Ar($\tilde{A}$) dissociation threshold, the energy required is ΔE_{E-A} plus the energy shortfall between the photolysis photon energy and the $\tilde{A}-\tilde{X}$ dissociation threshold. Because the P branch transitions occur at longer wavelengths, at photolysis energies below threshold probing via the P branch does not excite NO–Ar above the dissociation onset within the $\tilde{E}$ state. However, this is not the case for the shorter wavelength R branch. At threshold, the NO–Ar $\tilde{E}$ state dissociation is accessed at the (absent) Q band position of the NO $E \leftarrow A$ transition, while for $E_a=-12$ cm^{-1} it is accessed 12 cm^{-1} to the blue. Interestingly, the $E_a=0$ cm^{-1} spectrum clearly shows the sharp onset of a background at the expected (absent) Q band position, while for $E_a=-12$ cm^{-1} the onset is gradual, starting just above the (absent) Q band position excitation and rising to a plateau by $R(2)$. As will be discussed in Sec. IV, this suggests that the population is spread across a range of energies within the $\tilde{X}$ state of the complex.

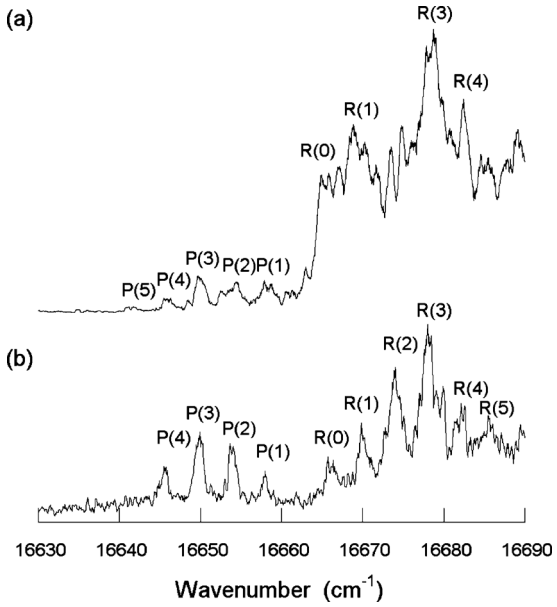

FIG. 2. REMPI spectra showing the $E \leftarrow A$ transition for NO A products formed following photolysis of NO–Ar at the laser excitation positions (a) 44 287 and (b) 44 275 cm^{-1}, associated with effective excess energies in NO–Ar of approximately 0 and −12 cm^{-1}, respectively. Note that the interference underlying the R branch is absent for the P branch.

Because of this interference, the NO products for $E_a \leq 0$ cm^{-1} were probed via the P branch of the $E \leftarrow A$ transition. To ensure that the distributions obtained were due to A state NO products, spectra at $E_a=0$, −12, and also −23 cm^{-1} were obtained for the R branch of the $F \leftarrow A$ transition where the analogous interference is significantly reduced. The distributions obtained from these two probe channels were consistent. In both cases, transitions from $N=0$ cannot be observed.

The spectra in Fig. 1 confirm the observations of Parsons *et al.*[14] that for E_a in the range 100–25 cm^{-1} the NO product

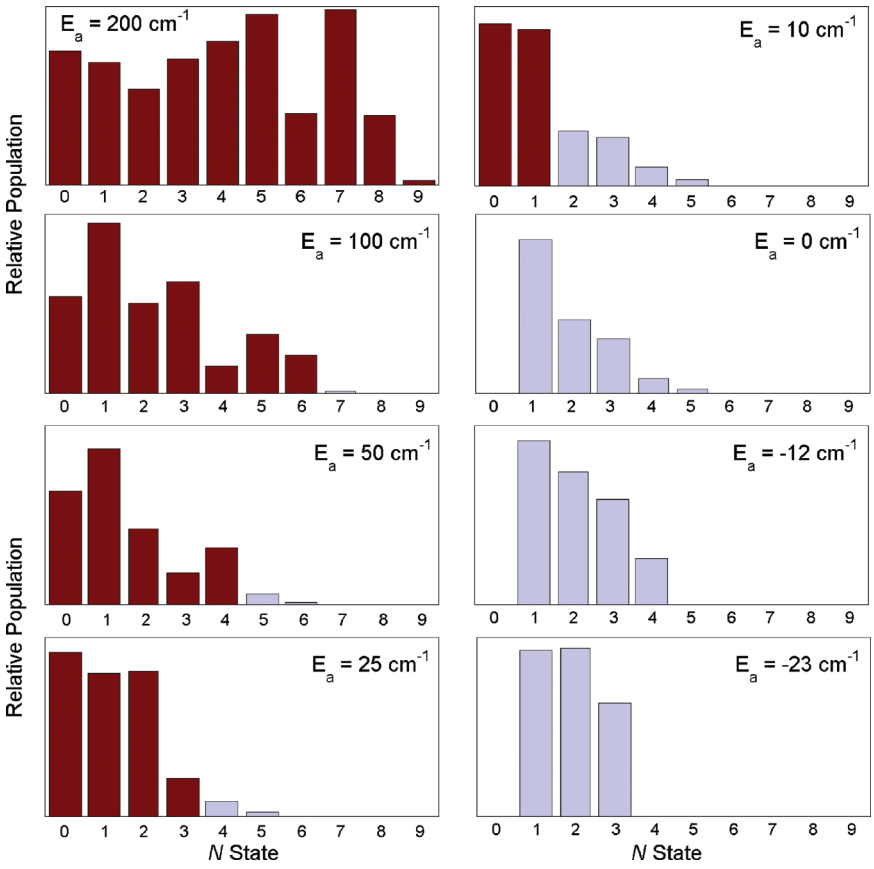

FIG. 3. The rotational population distributions extracted from the REMPI spectra for each of the photolysis wavelengths, as discussed in the text. The distributions are colored to show the energetically allowed (dark shade) and forbidden (light shade) rotational peaks, in the same fashion as those presented by Parsons *et al.* (Ref. 14). Note that $N=0$ could not be observed for $E_a \leq 0$ (see text).

is produced with more rotational energy than is expected to be available to the products. Moreover, as seen in Fig. 2, we find that this effect continues to lower energies, with products observed following excitation that is below the dissociation threshold. Population is observed in NO N states that should be "energetically inaccessible."

Relative rotational population distributions were extracted from the spectra as follows. Each spectrum was fitted to a sum of Gaussians, with the coefficient of the Gaussian for each peak providing the contribution of the corresponding rotational transition to the spectrum. The relative population in each N state was extracted from the spectral contribution by accounting for the intrinsic intensity differences (Hönl–London factors).[20] The resulting rotational population distributions are shown in Fig. 3. Based on the E_a values, a number of the N states observed should be inaccessible. The distributions shown in Fig. 3 identify the contributions from accessible and inaccessible N states, allowing comparison with those observed by Parsons *et al.*[14]

B. Translational energy distributions

To ascertain the total energy in the products, the translational energy distribution for each NO N state product is measured. In excess of 60 product state velocity map images were acquired, along with additional background images at each of the 8 photolysis energies.

Ignoring the NO A state electronic energy, the products of NO–Ar dissociation have rotational (NO only) and translational energy (NO and Ar), with the NO and Ar translational energies related by conservation of momentum. For a given amount of energy available to the products, the translational energy of a particular NO N state is fixed at

$$E_{\text{Translation}}^{\text{NO}} = \frac{m_{\text{Ar}}}{m_{\text{NO}} + m_{\text{Ar}}}(E_a - E_{\text{Rotation}}(N)).$$

Examples of translational energy distributions are shown in Fig. 4. For energetically accessible N states, we find that the distributions show not only the expected peak but also a "tail" extending to high translational energy. In general, the prominence of the tail decreases with increasing available energy. The distributions for energetically inaccessible states do not show a peak. They have a similar shape to the tail seen in the distributions of the energetically accessible N states.

IV. DISCUSSION

A. Source of the NO signal

The experiment detects NO(A) present 300 ns following a UV pulse tuned to various wavelengths in the region of NO–Ar $\tilde{A} \leftarrow \tilde{X}$ absorption. Since we observe NO(A) products that have more energy than expected, it is important to eliminate, as far as possible, species other than NO–Ar as the source.

While spectroscopic investigations have revealed broad features that have been attributed to larger complexes,[4,5,8,9] dissociation from such complexes following UV excitation has not been reported as problematic in past experimental explorations of NO–Ar $\tilde{A}$ dissociation. None of the previous reports probing the NO(A) products have reported interfer-

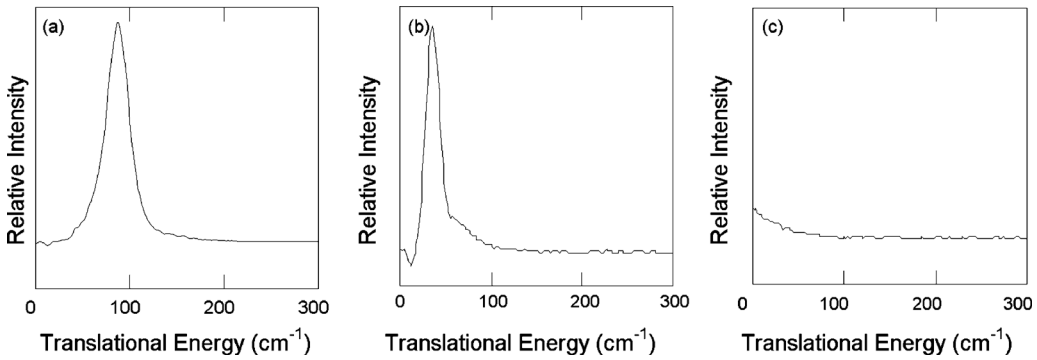

FIG. 4. Typical translational energy distributions extracted from velocity map images of rotational state-selected NO A products at several photolysis wavelengths: (a) photolysis at 44 487 cm^{-1} (E_a=200 cm^{-1}), monitoring NO via $R(7)$, (b) photolysis at 44 337 cm^{-1} (E_a=50 cm^{-1}), monitoring NO via $R(2)$, and (c) photolysis at 44 275 cm^{-1} (E_a=−12 cm^{-1}), monitoring NO via $P(3)$.

ence from this source, including Parsons *et al.* who first observed population in energetically inaccessible NO N states.[14] In our earlier paper on dissociation at E_a=50 cm^{-1}, we reported on our investigations into alternative sources for the NO A state products.[16] We showed the following.

(a) Background velocity map images, taken with both photolysis and probe lasers present but the probe laser detuned from an $E \leftarrow A$ NO rotational feature, enable us to rule out residual NO or alternative excitation/dissociation pathways involving NO–Ar as a source.
(b) Velocity map images taken at wavelengths where NO–Ar is observed to dissociate but with the apparatus tuned to the NO–Ar mass reveal no signal beyond the beam velocity. Such signal would be expected if excitation and subsequent sequential dissociation of higher $NO-Ar_n$ clusters were producing the NO responsible for the observed distributions.
(c) Investigation of the $NO-Ar_2 \rightarrow NO+Ar_2$ dissociation mechanism found no evidence for this as a source of NO.

In the present set of experiments we have also explored the possibility that the NO arises from dissociation of a larger NO cluster. The NO dimer is known to dissociate at much higher energies than are accessed here,[21] however, it is possible that a larger cluster may involve a weaker bond. Excitation of a beam of NO seeded in He at the same NO fraction and backing pressures used in our NO/Ar expansion does not show the NO features that we detect in the Ar beam. With the caveat that the kinetics of formation of NO clusters are similar in He and Ar, this effectively eliminates NO clusters as the source of the signal.

Experimentally, we have found no evidence for the involvement of $NO-Ar_n$ $(n>1)$ or $(NO)_n$ $(n>1)$ clusters in generating the NO A signals. The possible role of higher Ar clusters, $NO-Ar_n$ $(n>1)$, can also be shown to be highly unlikely through examination of the energetics. In the case of NO–Ar, the excitation energy $h\nu$ and the energy available to the products are related by

$$E_a = h\nu - (E_{\mathrm{NO}\ A-X} + D_0^0(\mathrm{NO-Ar})),$$

where $E_{\mathrm{NO}\ A-X}$ is the energy difference between the zero point energies of the NO A and X states and $D_0^0(\mathrm{NO-Ar})$ is the binding energy for NO–Ar in the $\tilde{X}$ state, measured from the zero point energy. Bare NO is monitored as the product in our experiment. For dissociation of $NO-Ar_n$ $(n>1)$ clusters to form NO, there are three possible processes.

(1) The first, which represents one limit, involves complete dissociation of the cluster to form NO and Ar atoms: $NO-Ar_n \rightarrow NO+nAr$. In this case, the available energy is

$$E_a = h\nu - (E_{\mathrm{NO}\ A-X} + E_{\mathrm{binding}}(\mathrm{NO-Ar_n})),$$

where $E_{\mathrm{binding}}(NO-Ar_n)$ is the binding energy for the cluster, i.e., is the minimum energy (excluding possible barriers) associated with the process $NO-Ar_n \rightarrow NO+nAr$. Since $NO-Ar_n$ $(n>1)$ clusters can only form if $E_{\mathrm{binding}}(NO-Ar_n) > D_0^0(NO-Ar)$, the threshold for complete dissociation of the cluster occurs at higher energy than the NO–Ar dissociation threshold and there is less energy available to the products. The dissociation products are observed to have more rotational and translational energies than expected for NO–Ar dissociation, which cannot be explained by this mechanism.
(2) The second possible process, and opposite limit to case (1), is $NO-Ar_n \rightarrow NO+Ar_n$. In this case, the available energy is larger than for case (1) by the binding energy of the Ar_n product,

$$E_a = h\nu - (E_{\mathrm{NO}\ A-X} + E_{\mathrm{binding}}(\mathrm{NO-Ar_n}) - E_{\mathrm{binding}}(\mathrm{Ar_n})).$$

In the case where $E_{\mathrm{binding}}(NO-Ar_n) - E_{\mathrm{binding}}(Ar_n) > D_0^0(NO-Ar)$, the threshold for this process occurs at higher energy than the NO–Ar dissociation threshold, inconsistent with this being the source. Only in the case where $E_{\mathrm{binding}}(NO-Ar_n) - E_{\mathrm{binding}}(Ar_n) < D_0^0(NO-Ar)$, i.e., $E_{\mathrm{binding}}(NO-Ar_n) - E_{\mathrm{binding}}(Ar_n) < 96$ cm^{-1}, is E_a larger than it is for the case of NO–Ar. The velocity map images allow us to determine limits on the energies associated with these processes since we can determine the total translational energies associated with the NO velocities observed assuming the process to be

$$NO - Ar_n \rightarrow NO + Ar_n.$$

The minimum possible energy available in the $NO\text{-}Ar_n \rightarrow NO + Ar_n$ dissociation is the sum of the maximum translational energy observed and the corresponding NO rotational energy, which assumes the Ar_n rotational and vibrational energies to be zero at the maximum translational energy. For example, in the case where $E_a = 0$ for NO–Ar, from the NO velocities observed for each NO N product, the range of available energies associated with different values of n can be calculated. We find that to form NO in the $N=4$ rotational level, the excess energy must, as a minimum, lie in the range 75–87 cm^{-1}, where the lower value is for $n=2$ and the higher value is the limit for large n.

From the discussion above this implies that for $n=2$,

$$E_{binding}(NO - Ar_2) - E_{binding}(Ar_2) < D_0^0(NO - Ar) - 75 \ cm^{-1},$$

$$\text{i.e.,} \ E_{binding}(NO - Ar_2) - E_{binding}(Ar_2) < 21 \ cm^{-1}.$$

From the Ar_2 well depth and zero point energy reported by Herman *et al.*,[22] $D_0^0(Ar_2)$, i.e., $E_{binding}(Ar_2)$, is 84.5 cm^{-1} and thus $E_{binding}(NO-Ar_2) < 105.5$ cm^{-1}. Recalling that $E_{binding}(NO-Ar_2)$ is the binding energy associated with the process $NO\text{-}Ar_2 \rightarrow NO + 2Ar$, with $D_0^0(NO-Ar) = 96$ cm^{-1} it seems highly unlikely that the bonding of a second Ar lowers the energy by <10 cm^{-1}.

At the other extreme, large n, we have $E_{binding}(NO-Ar_n) - E_{binding}(Ar_n) < 9$ cm^{-1}. As noted above, $D_0^0(Ar_2)$ is 84.5 cm^{-1}, of similar magnitude to $D_0^0(NO-Ar)$ which is 96 cm^{-1}. Thus one might expect that $E_{binding}(NO-Ar_n)$ is similar to $E_{binding}(Ar_{n+1})$. The left hand side of the inequality above is thus likely to be of the same magnitude as the binding energy of a further Ar to Ar_n. Given the Ar_2 binding energy of 85 cm^{-1}, this is unlikely to be less than 9 cm^{-1}. Consequently, the energetics suggest that it is extremely unlikely that dissociation of clusters via $NO-Ar_n \rightarrow NO + Ar_n$ is responsible for the NO signal observed.

(3) A third possibility is that a mechanism of the type $NO-Ar_n \rightarrow NO + Ar_{n-m} + Ar_m$ occurs, either stepwise or concertedly. The formation of two smaller Ar clusters requires breaking more bonds than in case (2) above. Given that the energetics for $NO-Ar_n \rightarrow NO + Ar_n$ are inconsistent with the observations, the additional energy required for this possibility effectively rules it out as a mechanism to explain the observations, based on the rotational energies observed alone.

Analogous arguments can be made for the influence of $(NO)_n\text{-}Ar_m$ $(n+m \geq 3)$ complexes.

In summary, the evidence overwhelmingly supports the proposition that the NO(A) products monitored are produced from photodissociation of $NO-Ar(\tilde{A})$, a conclusion also reached by previous authors.[14]

B. The $\tilde{A}$ state dissociation energy, the observed dissociation onset, and the average initial thermal energy

As our experiment observes dissociation near threshold, it is clearly essential to know the dissociation energy accurately since this, in combination with the photon energy, is a key determinant of the energy available to the products. There have been three reports of the dissociation energy. Tsuji *et al.*[8] used action spectra to ascertain the onset of NO–Ar $\tilde{A}$ state dissociation, which they determined to be $44\,286.7 \pm 0.3$ cm^{-1}, while Parsons *et al.*,[14] using ion imaging, determined a value of $44\,291 \pm 2$ cm^{-1}. Most recently, Roeterdink *et al.*[10] have analyzed velocity map images of state-selected NO products produced from excitation of NO–Ar resonance bands above dissociation and have determined that the presence of population in several of the low-lying NO–Ar $\tilde{X}$ states has compromised the earlier measurements. Roeterdink *et al.*[10] have refined the appearance energy for the formation of $\tilde{A}$ state NO from the lowest $\tilde{X}$ state of NO–Ar to be $44\,294.3 \pm 1.4$ cm^{-1}, amounting to an 8 cm^{-1} increase in the dissociation energy over that determined by Tsuji *et al.*[8] The lower values reported earlier[10,14,16] are attributed by Roeterdink *et al.*[10] to excitation from low-lying $\tilde{X}$ states that have significant population in the expansion.

The study by Roeterdink *et al.*[10] has shown that the spread of population over a number of low-lying levels of the NO–Ar complex affects the dissociation energetics observed. We refer to this population distribution as the "beam temperature" distribution, since it is likely to be a nearly thermal distribution typical of those obtained in supersonic expansions. We refer to the lowest rotational level of the ground vibrational state generically as the $(J''=0, v''=0)$ level.

The results of Roeterdink *et al.*[10] show that the effect of the beam temperature distribution is to lower the observed dissociation energy from the value associated with excitation from the $(J''=0, v''=0)$ level. Thus, one can measure an "effective" dissociation energy for the experimental conditions that accounts for the average effect of the additional energy available from the beam temperature distribution. We have done this using a series of velocity map images of NO products in individual N states arising from dissociation of NO–Ar at $E_a \sim 200$ cm^{-1}. This value is chosen because the accuracy of the result is increased when a significant number of N states are used. As noted in Sec. III B, the translational energy distributions show a peak at the position corresponding to the difference between the photon energy and the sum of the NO product rotational energy and NO–Ar dissociation energy. Plotting the position of the translational energy peak for each N state as a function of the rotational energy allows E_a to be determined for our expansion conditions, from which the dissociation energy is determined. The dissociation energy so derived is $44\,287.0 \pm 0.5$ cm^{-1}, some 7 cm^{-1} below the value inferred from the results of Roeterdink *et al.*,[10] indicating an effective average NO–Ar internal energy of approximately 7 cm^{-1} for our beam temperature distribution. Our value is in close agreement with that of Tsuji

TABLE I. The energy in excess of E_a that is required in $\tilde{A}$ state NO–Ar in order to produce the highest N state of the NO A product observed at each E_a probed.

E_a (cm^{-1})	Additional energy (cm^{-1})
−23	47
−10	52
0	60
10	50
25	35
50	34
100	12
200	0

et al.[8] (44 286.7 ± 0.3 cm^{-1}), suggesting that our expansion conditions produce an NO–Ar internal temperature very similar to the one produced by those authors. Under our experimental conditions, the average excitation energy relative to the true dissociation energy [i.e., for excitation from ($J''=0$, $v'=0$)] is 7 cm^{-1} higher than the photolysis photon energy since the molecules start with 7 cm^{-1} internal energy on average. Because our experiments do not probe the resonance features seen above dissociation, we are unable to comment on the revised dissociation energetics inferred by the results of Roeterdink *et al.*[10]

C. $\tilde{X}$ state contributions to photolysis at the onset of $\tilde{A}$ state dissociation

The experimental data reveal population in NO N states that are inaccessible based on excitation from ($J''=0$, $v'=0$). However, as we have discussed, Roeterdink *et al.*[10] have shown that the NO–Ar $\tilde{X}$ population is distributed over a range of states and this produces NO–Ar $\tilde{A}$ at higher energies for a given photolysis wavelength than is produced from ($J''=0$, $v'=0$). A key issue in the context of our results is the energy to which the $\tilde{X}$ state population distribution must extend to explain our observations.

At each value of E_a, the rotational energy of the highest observed NO N state gives a lower bound to the additional NO–Ar internal energy required to produce this product. Hence, the minimum $\tilde{X}$ state energy from which the excitation originates may be deduced. Table I lists the energies, additional to E_a, that were necessarily present in $\tilde{A}$ state NO–Ar in order to produce the highest N state observed at each E_a probed. It shows that states up to 60 cm^{-1} in the $\tilde{X}$ state of NO–Ar contribute to the observed rotational products. This value is significantly above the 7 cm^{-1} average thermal energy.

The evidence from the rotational distributions is, therefore, that $\tilde{X}$ vibrational states with at least 60 cm^{-1} energy can be excited to the $\tilde{A}$ state and contribute to the observed dissociation in the threshold region. While the rotational distributions provide a lower bound to the energy of the states involved, the rotational states may also be formed with translational energy. The translational energy distributions can be used to extract an upper bound. By obtaining the maximum translational energy for each rotational product state, the maximum energy in the dissociating molecule can be determined. Plotting the translational energy distributions for each E_a, shifted to account for the rotational energy of the N state probed, causes the distributions to become aligned to a common energy cutoff, showing that the maximum energy available is the same for all N. The tails all have the same shape and lie on top of each other when scaled vertically and shifted in energy to account for the N state's rotational energy. Examples of such plots are shown in Fig. 5 for E_a = 25 and 50 cm^{-1}. Using the values for all E_a, we determine that the translational energy distributions cutoff of approximately 94–106 cm^{-1} above each E_a. As the dissociation energy of NO–Ar in the $\tilde{X}$ state, derived from the appearance energies reported by Roeterdink *et al.*,[10] is 96 cm^{-1}, and given that resolution limitations broaden the distribution, the cutoff in the distributions is consistent with this available excess energy.

The translational energy distributions suggest that, despite the low temperature of the supersonic expansion, some population is retained in states up to the dissociation limit in the NO–Ar complex and these states are contributing to the dissociation dynamics observed. Further analysis of the distributions allows us to determine the degree to which population from the higher-lying $\tilde{X}$ vibrational states is contributing to each NO rotational state population. The peak in the translational distributions arises from excitation of low-lying vibrational states, i.e., those encompassed by the beam temperature distribution. The tail arises from higher-lying states for which vibrational cooling is incomplete. For each E_a, the areas of the peak and tail for an N state translational energy distribution reveal the relative contributions to that N state population from the beam temperature distribution and the higher-lying $\tilde{X}$ vibrational states. These are shown in Fig. 6. The contribution from the higher-lying $\tilde{X}$ vibrational states is significant near the dissociation threshold, and decreases with increasing E_a, becoming minimal at 200 cm^{-1}, the highest E_a investigated. This observation, seen here for a set of data spanning a substantial range of E_a, is consistent with our previously reported observation from E_a=50 cm^{-1}.[16]

D. How can $\tilde{X}$ states with low population contribute significantly to $\tilde{A}$ state dissociation?

Spectra of cold NO reveal our beam rotational temperature to be ~1.0 K and, as discussed in Sec. IV B, the NO–Ar beam temperature distribution has an average energy of 7 cm^{-1}, as determined from the shift in dissociation energy. However, both the rotational and translational distributions of the NO products indicate that $\tilde{X}$ states at higher energies, up to the dissociation limit, contribute to the $\tilde{A}$ state dissociation near threshold, in spite of the low populations that the temperature and average energy infer. We suggest that the reason for the importance of these states lies in an increase in the transition moment for them, with an increase in the Franck–Condon factors for the excitation process the most reasonable explanation. Recent calculations[23] confirm that the NO–Ar $\tilde{X}$ state has a "T" structure,[3] while the $\tilde{A}$

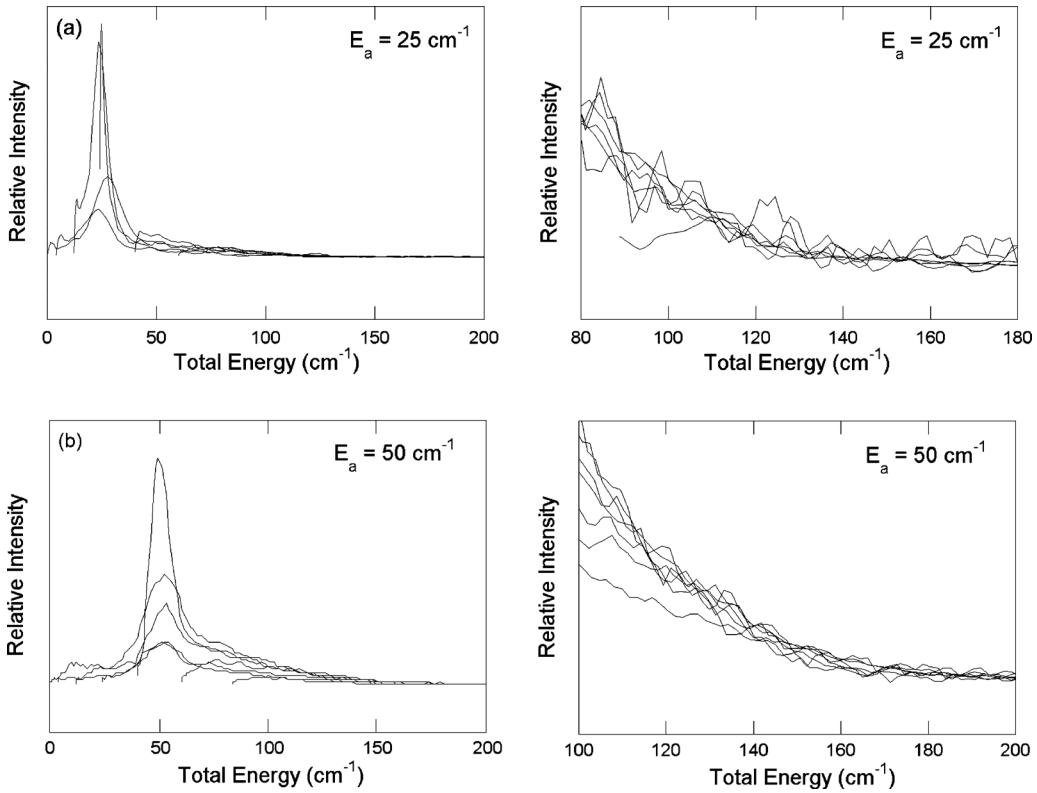

FIG. 5. Translational energy distributions measured for the set of NO N state products at (a) E_a=25 cm^{-1} and (b) E_a=50 cm^{-1}, shifted to account for the rotational energy of the N state probed. At each E_a the distributions align to a common energy cutoff, showing that the maximum energy available is the same for all N.

state is near linear.[6] The NO–Ar bond length is substantially increased from the $\tilde{X}$ to $\tilde{A}$ states.[3,6,23] There is, therefore, poor overlap between the ground vibrational levels in the two electronic states. Indeed, this led to the bound-bound transitions remaining unobserved for some time.[1,7] The poor Franck–Condon overlap is illustrated by the results of Shafizadah *et al.*[5] who estimated the bound-bound transitions to be over two orders of magnitude weaker than the bound-free transitions. However, the overlap improves in vibrational modes that allow access to regions where the two states have common geometry. The high amplitude motions of higher vibrational levels in the NO–Ar ground state provide improved overlap with the excited electronic state. Thus, while we expect there to be very low population in these states in the expansion, we propose that, in the region we are probing, transitions between these and the $\tilde{A}$ state are significantly more intense. In this case, it is the product of the population and Franck–Condon factor that is important, with the much larger Franck–Condon factors making high energy vibrational states with low population observable. The shape of the tails in the translational energy distributions (see Figs. 4 and 5) indicates the fraction of the population initially produced at each $\tilde{A}$ state excess energy, which is a product of the $\tilde{X}$ state population distribution and the Franck–Condon factors for the appropriate transitions. As we have noted above (see Fig. 5), for a given photolysis energy the tails have the same shape, consistent with a common initial distribution.

We note that the formation mechanism for van der Waals complexes involves a three-body collision, where the third body removes excess energy, reducing the energy in the remaining two bodies to below the dissociation energy for the complex, forming the van der Waals molecule. Further collisions are generally required to cool the complex to the lowest states. It is, thus, not surprising that some population remains in the higher-lying states, just as a small population remains in higher-lying rotational states of NO following collisional cooling during the supersonic expansion. This has been explored in detail by Zacharias *et al.*[24] and the effect is illustrated, for example, by the NO rotational structure seen in Langridge–Smith's original NO–Ar spectrum.[1]

It follows from our rationalization of the experimental results that the tails of the translational energy distributions reflect the product of the population distribution in the $\tilde{X}$ state of NO–Ar and the Franck–Condon factors for excitation from these $\tilde{X}$ states to energies above dissociation in the $\tilde{A}$ state. To determine either the Franck–Condon factors or the population distribution requires knowledge of either one or the other, which we do not have. However, if one is able to make a reasonable (order of magnitude) estimate of, say, the population distribution, then one can see whether the Franck–Condon factors so obtained are reasonable and, hence, whether our proposition is reasonable.

While there are no population data available for the NO–Ar complex, population distributions have been measured for NO in a supersonic expansion.[24] These distributions reveal population in higher rotational states, trapped when cooling stops as the collision frequency drops with

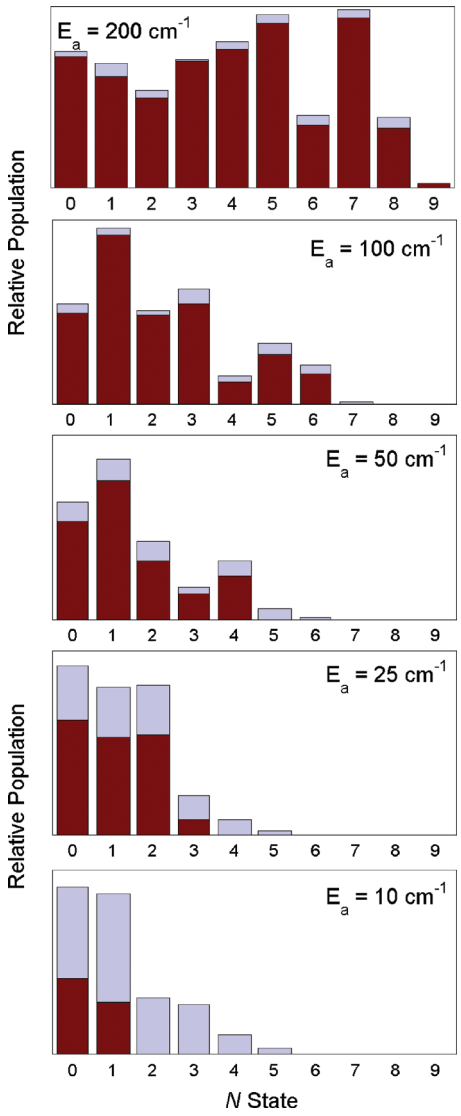

FIG. 6. Rotational population distributions showing the relative contributions to each N state population from the beam temperature distribution (dark shade) and higher-lying $\tilde{X}$ vibrational states (light shade) for $E_a \geq 10$ cm^{-1}. For values of $E_a \leq 0$ cm^{-1}, only the higher-lying $\tilde{X}$ vibrational states contribute, as is shown in Fig. 3.

increasing distance from the nozzle. We recognize that the NO–Ar vibrational distribution is unlikely to match the NO rotational distribution, but in the absence of other information it provides a starting point for estimation and illustration. We have fitted the observed NO rotational distribution up to ~100 cm^{-1} to a functional form and assumed this functional form to represent the NO–Ar $\tilde{X}$ vibrational population distribution. Over the energy range 0–100 cm^{-1}, this estimate suggests that the population decreases by approximately three to four orders of magnitude.

The tails of the translational energy distributions represent the product of the population and Franck–Condon factors. Using the NO–Ar population distribution extracted as discussed in the preceding paragraph, the Franck–Condon factors for accessing a particular range of the $\tilde{A}$ state can be determined. Using the tails for the translational energy distributions for E_a=50 cm^{-1}, we have extracted Franck–Condon factors. The Franck–Condon factors determined are predicted to be approximately two orders of magnitude larger for highly excited $\tilde{X}$ states compared with the ground state. This is, of course, simply indicative as it relies on a highly uncertain population distribution. Nevertheless, it suggests that the changes in the magnitude of the Franck–Condon factors required are not unreasonable. Shafizadeh *et al.*[5] have pointed out that the excitation moment decreases by almost three orders of magnitude from the bound-free to the bound-bound transitions.

E. Spectral observation of high-lying NO–Ar $\tilde{X}$ states

A natural question to arise when considering our explanation for the experimental observations is: why, if this explanation is correct, transitions from the higher-lying $\tilde{X}$ states have not been observed in studies of the $\tilde{A} \leftarrow \tilde{X}$ spectrum? Of course, hotband transitions have been reported, which identify transitions from several $\tilde{X}$ states with energies up to 27 cm^{-1}.[4,9,15,25]

Examination of the literature reveals that spectra of the bound region of the NO–Ar $\tilde{A} \leftarrow \tilde{X}$ transition show unusual behavior. The reports by McQuaid *et al.*,[9] Bush *et al.*,[4] and Shafizadeh *et al.*[5] are particularly revealing as they report spectra taken under various conditions. Certain experimental conditions produce the features that are now well established as belonging to NO–Ar. Spectra taken under different conditions show additional features, with little commonality among the spectra reported by the three groups. McQuaid *et al.*[9] and Bush *et al.*[4] are clearest in identifying the experimental conditions. Both find that spectra taken earlier in the pulse, where conditions are coldest,[4] produce the usual NO–Ar spectrum; later spectra show additional features. These two groups use mass resolved REMPI spectroscopy to observe the spectrum at the NO–Ar mass. Shafizadeh *et al.*[5] do not specify the different conditions used. Their spectra are taken using Laser Induced Fluorescence (LIF) and are not mass selective.

McQuaid *et al.*[9] reported additional features between approximately 44 180 and 44 260 cm^{-1} (the origin band is at 44 242 cm^{-1}) for their "later in the pulse" spectra, i.e., the additional features are predominantly to the red of the origin band. While some structure is seen, it appears on top of a broad underlying background. The authors ascribe these features to $Ar_n(NO)_m$ $(n+m \geq 3)$. In contrast, Bush *et al.*[4] reported additional features analogous to those seen in Miller's original spectrum,[25] consisting of "an irregular series of broad, unresolved features extending to lower wavenumber than observed in our other experiments." Examination of their spectrum suggests that these features are most prominent below 44 270 cm^{-1}. They ascribe the additional features either to excitation from vibrationally excited NO–Ar or to excitation and fragmentation of larger NO–Ar containing clusters. In contrast to McQuaid *et al.*[9] and Bush *et al.*,[4] Shafizadeh *et al.*[5] observed growth at the blue end of the bound spectrum. This growth is by way of a broad, unstruc-

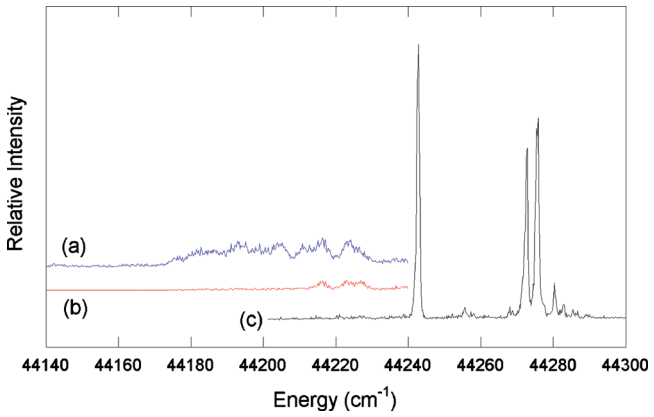

FIG. 7. (1+1) REMPI spectra acquired at the NO–Ar mass. Traces are (a) the total ion counted signal, (b) the ion counted signal in the center of the image, and (c) the integrated signal on the CCD camera. Note the broad feature, predominantly red shifted from the origin, which we attribute to larger clusters.

tured background that increases in intensity as the laser excitation moves to the blue. They ascribe this signal to "a larger complex."[5]

It is particularly noteworthy that McQuaid *et al.*[9] and Bush *et al.*[4] do not see the additional structure at the blue end of the spectrum reported by Shafizadeh *et al.*[5] As we have shown in Sec. IV A, the energetics derived from the NO translational and rotational energies observed do not support dissociation of larger clusters to form NO in this higher energy region.

To try to resolve these inconsistencies, we have examined the (1+1) REMPI spectrum at the NO–Ar mass using velocity and mass resolution, the so-called VMR-REMPI.[26] We have shown previously[26] that one can easily distinguish parent from offspring ions in such an experiment because the parent ions only appear at the image center, since they have no orthogonal momentum component as occurs for dissociation products. This provides a means to assign whether the signal observed at the NO–Ar mass originates from NO–Ar or from higher clusters that have undergone dissociation. The spectrum was measured with high sensitivity using ion counting and, unlike the spectra referred to above, was taken under conditions where the cold NO–Ar spectrum is maximized.

The measured spectrum is shown in Fig. 7. In addition to the usual NO–Ar spectrum, it reveals a weak, broad feature, primarily to the red of the origin band and extending some 60–65 cm^{-1} to lower energy. There are several peaks distinguishable, and these correspond to the hotbands previously assigned.[15] The spectrum is very similar to that reported by McQuaid *et al.*[9] Analysis of the high and low velocity components of the images reveals a high velocity component to the broad feature. It is thus associated with dissociation of larger clusters, $Ar_n(NO)_m$ $(n+m \geq 3)$. We scanned the same spectral region while monitoring the $NO-Ar_2$ mass and no signal was observed, suggesting that if this is the source then it dissociates with 100% efficiency. Examination of the images reveals significant translational energy in the products (approximately hundreds of cm^{-1}). In combination with the discussion in Sec. IV A, this indicates that dissociation of these larger clusters is occurring from the cation complex. Our spectrum reveals that the contribution of larger NO–Ar complexes to the REMPI spectrum at the NO–Ar mass is predominantly to the red of the origin band, with a diminishing contribution up to ~24 cm^{-1} to the blue of the origin band. Given the almost halved well depth in the exited versus the ground state, it is in this region where one might hope to see hot and sequence bands, however, such transitions are masked by the presence of clusters in our spectrum. There are features seen, particularly by Bush *et al.*,[4] that are additional to those seen in our spectrum and these may be due to excitation from higher states of $NO-Ar\,\tilde{X}$ under their warmer conditions, which is a possibility they suggested.

The LIF spectra of Shafizadeh *et al.*[5] provide support for the explanation we have proposed to rationalize our observations. Due to interference from uncomplexed NO, they did not extend the spectrum to the red of the origin band and so did not observe the features associated with larger clusters discussed above. Interestingly, there is no growth just to the blue of the origin band as is observed in our spectrum, suggesting that large clusters are not a significant contributor under their experimental conditions, although the signal to noise ratio in their spectra may preclude its observation. Their sequence of spectra (see Fig. 2 of their paper) shows a broad background at the blue end of the spectrum whose intensity is dependent on the expansion conditions. While they attribute this to emission from larger clusters, the observations of cluster absorption discussed above lead us to suggest that it could be due to excitation and dissociation of NO–Ar and the change in its intensity comes from increased population of higher $\tilde{X}$ states under some expansion conditions. This interpretation provides a consistent picture of the NO–Ar spectrum, the onset of dissociation of the complex and the role of higher $\tilde{X}$ states in that process, and the spectral manifestations of larger clusters.

F. Rotational population maxima and the rainbow effect

Our NO N state relative rotational population distributions display the rotational rainbow effect previously reported.[12] As was the case in these earlier studies, our rotational populations show two maxima for $E_a \geq 50$ cm^{-1}. These are independent of contributions from the population in higher $\tilde{X}$ state levels. Both the lower and upper N_{max} states vary with E_a. In a number of instances our values differ from those reported by Parsons *et al.*[14] by one N value (see Fig. 8). Because our scans are of higher resolution, it is likely that we have been better able to determine the N_{max} values. Although the values differ slightly, both sets of results support the relationship of proportionality between N_{max} and $\sqrt{E_{available}}$, consistent with the original findings of Sato *et al.*[12]

G. Consistency with previous measurements

Since there have been several measurements of NO–Ar dissociation from the $\tilde{A}$ state, before concluding we consider

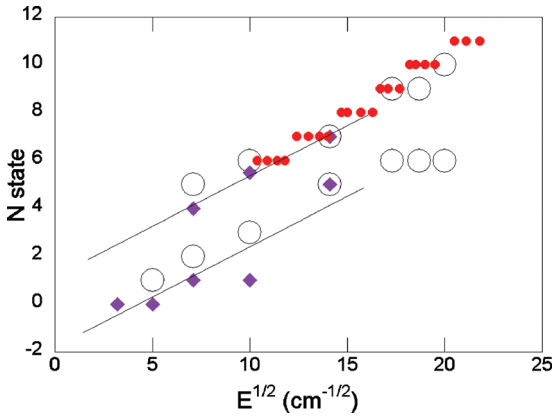

FIG. 8. Plot of N_{max} vs $\sqrt{E_{available}}$, where N_{max} is the N value at which the distribution peaks. Because the distribution is bimodal for $E_a \geq 50$ cm^{-1}, there are two values of N_{max}, corresponding to the low and high sections of the distribution. The data points are small dots [Sato *et al.* (Ref. 12)]; open circles [Parsons *et al.* (Ref. 14)]; diamonds (our data).

the extent of the consistency or anomalies between observations by the different groups. There are four sets of measurements that we consider in turn.

In order to estimate the $\tilde{A}$ state dissociation energy, Sato *et al.*[12] examined the photolysis wavelength at which the $N=9$ NO product first appears. They probed in the range 44 472–44 460 cm^{-1}, corresponding to $E_a \sim 180$ cm^{-1}, and observed a sharp onset for $N=9$. Our rotational distribution for $E_a=200$ cm^{-1} shows almost negligible contribution from thermally populated levels at this E_a and, in fact, we detect no contribution from high energy $\tilde{X}$ levels to the $N=9$ population, consistent with Sato's results. The influence of population in the high $\tilde{X}$ levels diminishes with increasing E_a, as is expected since the Franck–Condon factors for transitions from the low energy $\tilde{X}$ levels (where the population is largest) increase with increasing $\tilde{A}$ state excitation energy (up to the Franck–Condon maximum).

Tsuji *et al.*[8] measured photodissociation action spectra for individual NO N states, determining the photolysis wavelength at which the NO signal first showed an increase in ionization signal. By measuring this onset for a range of NO N states, the dissociation energy was extracted. Population in high energy NO–Ar $\tilde{X}$ states could potentially confound that measurement by producing products at lower excitation energies than the dissociation onset, even accounting for the shift associated with the beam temperature distribution. The question is why this was not observed. The potential inconsistency is resolved by recognizing that ionization and consequent dissociation of NO–Ar by the photolysis laser lead to a background signal in Tsuji's spectra. We measured analogous action spectra using a 300 ns delay between the photolysis and probe pulses in order to remove the one laser background. These spectra reveal both a background below the $\tilde{A}$ state dissociation threshold and the expected increase in signal above threshold. This is consistent with both our measurements and the observations of Tsuji *et al.*[8]

Chandler's group has reported two sets of results. Initially, Parsons *et al.*[14] reported spectra of the NO products that reveal population in rotational states that should be inaccessible given the energy available; it is this result that inspired our investigations. While there are differences in detail (see Sec. IV F, for an example), the inaccessible NO N states we observe match those reported by these authors. Interestingly, as previously stated, Parsons *et al.*[14] reported a higher value for the dissociation energy than Tsuji *et al.*[8] or ourselves. Subsequently, Roeterdink *et al.*[10] reported REMPI spectra of the NO products produced by dissociation from resonances just above the dissociation threshold. Their two published spectra show population dominantly in the energetically allowed rotations, $N=0-2$, although their scan for excitation at 44 309.5 cm^{-1} reveals a small population in the $N=3$ state. Our spectra at comparable E_a values reveal population up to $N=5$. The major difference in these results arises because those of Roeterdink *et al.*[10] were obtained following excitation of specific NO–Ar transitions, while ours involve excitation into the continuum. The results of Roeterdink *et al.*[10] are thus significantly biased toward the products produced from the resonance. We note that their translational energy distributions (Figs. 3 and 4 of their paper) display not only the expected narrow peak but also the broad tail extending to high energy indicative of a contribution arising from excitation of higher levels of the $\tilde{X}$ state.

While there is broad consistency between our results and those of Chandler's group,[10,14] there are differences in detail. Specifically, (i) given the magnitude of the resonances compared with the background continuum, we might have expected a slightly larger contribution from energetically inaccessible NO N states than seen by Roeterdink *et al.*,[10] and (ii) Parsons' *et al.*[14] measurement of the dissociation energy, which would include the effect of the beam temperature distribution, is higher than the values Sato *et al.*[12] and we measure. Both results might arise if the expansion conditions used by Chandler's group are producing a colder NO–Ar distribution, with a reduced impact of higher $\tilde{X}$ states. In this context we note that our explanation for the experimental observations could be tested by experiments using expansion conditions that produce a colder internal distribution for NO–Ar. Such an experiment could be undertaken using, for example, a very high pressure pulsed valve such as the Evan–Lavie design,[27] although care would be required to ensure that NO–Ar remained the dominant species.

V. CONCLUSIONS

We have investigated the dissociation of $\tilde{A}$ state NO–Ar at effective excess energies in the range from −23 to 200 cm^{-1}. We find that there is a substantial contribution from population originating in high energy $\tilde{X}$ states of NO–Ar at the dissociation threshold, revealed through the population in NO product rotational states and in the translational energy distributions. The rotational distributions show population in states that are not accessible with the energy available for excitation from the NO ground vibrational level. This effect is observed at photon energies below the dissociation energy up to approximately 100 cm^{-1} above it. Translational energy distributions extracted from velocity map images reveal contributions from population in high energy $\tilde{X}$ states of NO–Ar at all the excess energies probed,

although it diminishes with increasing photon energy and is minimal at 200 cm^{-1}, the highest energy studied. The translational energy distributions show that there are contributions from vibrational levels extending up to the $\tilde{X}$ state NO–Ar dissociation energy. We propose that the reason for such significant contributions from sparsely populated levels is a considerable increase in the Franck–Condon factor associated with these highly excited states and this arises because of the quite different geometries in the NO–Ar $\tilde{X}$ and $\tilde{A}$ states.

ACKNOWLEDGMENTS

We thank the School's Electronic and Mechanical workshop staff for their support in constructing and maintaining the apparatus. This research was supported by the Australian Research Council and Flinders University.

[1] P. R. R. Langridge-Smith, E. Carrasquillo, and D. H. Levy, J. Chem. Phys. **74**, 6513 (1981).
[2] H. H. W. Thuis, S. Stolte, J. Reuss, J. J. H. van den Biesen, and C. J. N. van den Meijdenberg, Chem. Phys. **52**, 211 (1980).
[3] P. D. A. Mills, C. M. Western, and B. J. Howard, J. Phys. Chem. **90**, 4961 (1986).
[4] A. M. Bush, J. M. Dyke, P. Mack, D. M. Smith, and T. G. Wright, J. Chem. Phys. **108**, 406 (1998).
[5] N. Shafizadeh, P. Brechignac, M. Dyndgaard, J. H. Fillion, D. Gauyacq, B. Levy, J. C. Miller, T. Pino, and M. Raoult, J. Chem. Phys. **108**, 9313 (1998).
[6] J. Kłos, M. H. Alexander, R. Hernandez-Lamoneda, and T. G. Wright, J. Chem. Phys. **129**, 244303 (2008).
[7] J. C. Miller, J. Chem. Phys. **90**, 4031 (1989).
[8] K. Tsuji, K. Shibuya, and K. Obi, J. Chem. Phys. **100**, 5441 (1994).
[9] M. J. McQuaid, G. W. Lemire, and R. C. Sausa, Chem. Phys. Lett. **227**, 54 (1994).
[10] W. G. Roeterdink, K. E. Strecker, C. C. Hayden, M. H. M. Janssen, and D. W. Chandler, J. Chem. Phys. **130**, 134305 (2009).
[11] J. Lozeille, S. D. Gamblin, S. E. Daire, and T. G. Wright, J. Chem. Phys. **113**, 7224 (2000).
[12] K. Sato, Y. Achiba, H. Nakanura, and K. Kimura, J. Chem. Phys. **85**, 1418 (1986).
[13] R. Schinke, J. Chem. Phys. **84**, 1487 (1986).
[14] B. F. Parsons, D. W. Chandler, E. C. Sklute, S. L. Li, and E. A. Wade, J. Phys. Chem. **108**, 9742 (2004).
[15] O. L. A. Monti, H. A. Cruse, T. P. Softley, and S. R. Mackenzie, Chem. Phys. Lett. **333**, 146 (2001).
[16] H. L. Holmes-Ross and W. D. Lawrance, Chem. Phys. Lett. **458**, 15 (2008).
[17] J. R. Gascooke and W. D. Lawrance, J. Phys. Chem. A **104**, 10328 (2000).
[18] J. Luque and D. R. Crosley, J. Chem. Phys. **112**, 9411 (2000).
[19] E. W. Hansen and P.-L. Law, J. Opt. Soc. Am. A **2**, 510 (1985).
[20] G. Herzberg, *Molecular Spectra and Molecular Structure: 1 Spectra of Diatomic Molecules* (Van Nostrand Reinhold Company, New York, 1950); J. O. Hornkohl, C. G. Pariqqer, and L. Nemes, Appl. Opt. **44**, 3686 (2005).
[21] A. B. Potter, V. Dribinski, A. V. Demyanenko, and H. Reisler, J. Chem. Phys. **119**, 7197 (2003).
[22] P. R. Herman, P. E. LaRocque, and B. P. Stoicheff, J. Chem. Phys. **89**, 4535 (1988).
[23] Y. Kim, J. Fleniken, H. Meyer, M. H. Alexander, and P. J. Dagdigian, J. Chem. Phys. **113**, 73 (2000).
[24] H. Zacharias, M. M. T. Loy, P. A. Roland, and A. S. Sudbo, J. Chem. Phys. **81**, 3148 (1984).
[25] J. C. Miller and W. Cheng, J. Phys. Chem. **89**, 1647 (1985).
[26] R. K. Sampson, S. M. Bellm, J. R. Gascooke, and W. D. Lawrance, Chem. Phys. Lett. **372**, 307 (2003).
[27] U. Even, J. Jortner, D. Noy, N. Lavie, and C. Cossart-Magos, J. Chem. Phys. **112**, 8068 (2000).